Materials Transactions, Vol. 65, No. 1 (2024) pp. 18 to 26

Phase Equilibria in Aluminium–Ruthenium–Silicon System near 1200 Kelvin

Koichi Kitahara[1,2,*1], Hiroyuki Takakura[3], Yutaka Iwasaki[2,4,*2] and Kaoru Kimura[2,4,*3]

[1]*Department of Materials Science and Engineering, School of Electrical and Computer Engineering, National Defense Academy, Yokosuka 239-8686, Japan*
[2]*Department of Advanced Materials Science, Graduate School of Frontier Sciences, The University of Tokyo, Kashiwa 277-8561, Japan*
[3]*Division of Applied Physics, Faculty of Engineering, Hokkaido University, Sapporo 060-8628, Japan*
[4]*National Institute for Materials Science (NIMS), Tsukuba 305-0047, Japan*

A narrow-gap semiconductor with a complex crystal structure was recently discovered in the Al–Ru–Si system. To determine the homogeneity range of the semiconductor phase and further discover new phases, phase equilibria in the Al–Ru–Si system near 1200 K were investigated through prolonged-annealing experiments. Eleven new ternary phases including two incommensurate composite-crystalline and an icosahedral quasicrystalline phases were identified using powder and single-crystal X-ray diffraction, and their compositions at two-phase and three-phase equilibria were evaluated by means of electron-probe X-ray microanalysis. On the basis of the data obtained in this study and those adopted from the literature, a tentative isothermal section of the Al–Ru–Si equilibrium phase diagram near 1200 K was drawn.
[doi:10.2320/matertrans.MT-M2023128]

(Received August 16, 2023; Accepted October 16, 2023; Published December 25, 2023)

Keywords: *aluminium–ruthenium–silicon system, phase equilibrium, crystal structure, composition, prolonged annealing, X-ray diffraction, electron-probe X-ray microanalysis, matrix correction, incommensurate composite crystal, quasicrystal*

1. Introduction

Semiconductors with complex crystal structures have attracted interest primarily from thermoelectrics because an intrinsically low lattice thermal conductivity is expected for a complex-structure material.[1–4] Recently, a narrow-gap [approximately 24 zJ (0.15 eV)] semiconductor with a complex crystal structure (Pearson symbol ~*cP*31, i.e. approximately 31 atoms per unit cell) was discovered in the Al–Ru–Si system near the composition $Al_{67.6}Ru_{23.5}Si_{8.9}$[5] (referred to as the C phase following the nomenclature of Grushko and Velikanova[6]), and its thermoelectric properties were investigated through copper doping.[7] The lattice thermal conductivity of the C phase at temperatures above room temperature is approximately 1 $W\,m^{-1}\,K^{-1}$, which is as low as that of glass.[5,7] The carrier concentration in the C phase can be optimized through copper doping, but the bandgap seems to be narrowed simultaneously, which leads to a decrease in the thermopower compared to the one expected from theoretical calculations based on the rigid-band approximation.[7] The carrier concentration may be optimized without doping other elements, avoiding significant change in the bandgap, by changing the composition within the Al–Ru–Si system, but the phase equilibria involving and the homogeneity range of the C phase should be determined prior to such experiments.

In the binary Al–Ru and Ru–Si systems, there also exist narrow-gap semiconductors, i.e. $RuAl_2$ [Pearson symbol *oF*24,[8] bandgap (or pseudogap) of approximately 21 zJ (0.13 eV)[9]], RuSi(*cP*8) [*cP*8,[10] 42 zJ (0.26 eV)[11]] and Ru_2Si_3(*o*) [*oP*40,[12] 0.1 aJ (0.7 eV)[13]]. Given this fact, existence of other narrow-gap semiconductors in the Al–Ru–Si system is simply expected. However, information of ternary phases in this system was scarce. Only three ternary phases were found in the literature as described below.

Nowotny and coworkers[14–16] mentioned the $Ru(Al,Si)_{2-x}$ phase with the two compositions $Ru(Al_{0.2}Si_{0.8})_{2-x}$ and $Ru(Al_{0.5}Si_{0.5})_{2-x}$ (the value of x is not reported). Although the crystal structure (even the unit-cell parameters) was not determined completely, the $Ru(Al,Si)_{2-x}$ phase is considered a variant of the Ru_2Si_3(*o*) phase and hence falls into so-called Nowotny chimney ladder (NCL) phases,[17] which also include the $RuAl_2$ phase mentioned above. Since many NCL phases including the $RuAl_2$ and Ru_2Si_3(*o*) phases are semiconducting,[9,13,18,19] and the crystal structure of some NCL phases are complex,[20–22] $Ru(Al,Si)_{2-x}$ may also be a semiconductor with a complex crystal structure.

The C phase mentioned above was first discovered near the composition $Al_{69}Ru_{23}Si_8$ by Koshikawa *et al.*,[23] but only a powder X-ray diffraction (XRD) pattern was reported at that time. This phase was recently rediscovered in the course of searching for semiconducting quasicrystals and related crystals (so-called crystalline approximants) employing a band-engineering technique and confirmed to be a semiconductor.[5] The C phase is regarded as a cubic 1/0 rational crystalline approximant[24] to an icosahedral quasicrystal.[23] Since a quasicrystal and its approximants often exist in a close compositional region[6] and show similar transport properties,[25–27] there may exist semiconducting quasicrystalline and other approximant crystalline phases near the composition of the C phase.

Morrison *et al.*[28] grew some single crystals of $Ru_{23}(Al,Si)_{97}$ with compositions approximately ranging from $Al_{73}Ru_{20}Si_7$ to $Al_{68}Ru_{19}Si_{13}$ and determined its complex crystal structure (Pearson symbol *hP*240) using single-crystal XRD. Here, this phase is referred to as the χ' phase because the crystal structure is quite similar to that of the Ir_9Al_{28} phase (Pearson symbol ~*hP*222[29]), which is referred to as the χ phase in the nomenclature of Grushko and Velikanova.[6] The

*[1]Present address: National Defense Academy, Yokosuka 239-8686, Japan
*[2]Graduate Student, The University of Tokyo. Present address: National Institute for Materials Science (NIMS), Tsukuba 305-0047, Japan
*[3]Present address: National Institute for Materials Science (NIMS), Tsukuba 305-0047, Japan

χ' phase may be regarded as an approximant to a decagonal quasicrystal similarly to the χ phase.[29)]

Although the majority of the Al–Ru–Si system was unexplored, some phases with interesting characteristics had already been discovered as described above. In this study, phase equilibria in the Al–Ru–Si system near 1200 K were thoroughly investigated through prolonged-annealing experiments. The choice of 1200 K is a compromise between a lower annealing temperature and a shorter annealing time.

2. Methods

Alloy samples of desired nominal compositions were prepared from powders of aluminium (Kojundo Chemical Lab. Co., Ltd., Japan, 99.9 %), ruthenium (Tanaka Kikinzoku Kogyo K.K., Japan, 99.90 % or purer) and silicon (Kojundo Chemical Lab. Co., Ltd., Japan, 99.99 % or purer) using arc melting in an argon atmosphere (NEV-ACD-05, Nissin Giken Corporation, Japan). Each sample was then wrapped in a tantalum or graphite sheet, sealed in a silica tube filled with argon and annealed in a furnace at 1200 K for approximately from 114 h to 331 h, followed by water quenching. As this study was a long-term study spanning approximately a year (for annealing experiments only), the thermocouples of the furnaces could be deteriorated and damaged. During this study period, we repeatedly evaluated temperature deviations from the set temperature and temperature differences among different positions for each furnace using the Referthermo reference materials (Japan Fine Ceramics Center, Japan), and an uncertainty of at most 50 K or larger should be assumed for the annealing temperature. Samples that partly melt below 1200 K were placed in aluminium nitride crucibles instead of tantalum and graphite sheets. Samples for investigating phase equilibria were annealed at least twice to check for any significant changes in constituent phases and their unit-cell parameters by comparing powder XRD peak positions. This condition should imply equilibrium for most cases, but some samples remained nonequilibrium even in this condition, particularly for ruthenium-rich samples (see Secs. 3.1 and 3.4).

Depending on the alloy composition, samples can become highly inhomogeneous during solidification. To improve homogeneity, the following processes were used for some samples before annealing. Some samples were crushed into powders after melting and then compacted using pulsed electric current sintering with a uniaxial pressure of approximately 90 MPa in an argon atmosphere (SPS-515S, Sumitomo Coal Mining Co., Ltd., Japan). The maximum temperature during a sintering was approximately 1230 K or lower. Some other samples were prepared by just mechanically compacting powders without melting. Note that these processes were not always sufficient for improving homogeneity, and some samples remained inhomogeneous even after these processes (see Sec. 3.1 for examples).

Phases in the samples were identified using powder XRD (SmartLab, Rigaku Corporation, Japan; D8 ADVANCE, Bruker Corporation, USA; Cu K–$L_{2,3}$ radiation), and the composition of each phase was analysed by means of electron-probe X-ray microanalysis using the energy-dispersive spectrometer (EDS) equipped in a scanning electron microscope (SEM) (JSM-6010LA, JEOL Ltd., Japan). For the composition analyses, pure elemental substances (JEOL Ltd., Japan) were used as standard materials, and the Armstrong/Love–Scott model[30–32)] was used to correct for the matrix effects, which gives reasonable compositions for stoichiometric phases in the Al–Ru and Ru–Si systems (see Sec. 3.1 and Table 3). The unit-cell parameters were evaluated using the Le Bail method[33)] with the Jana2006 software[34)] for selected samples.

The crystal structure was determined using single-crystal XRD (XtaLAB Synergy-R, Rigaku Corporation, Japan; Mo K–$L_{2,3}$ radiation) if a sufficiently large single crystal could be obtained. Single crystals were either selected from crushed fragments of the samples described above or grown using the self-flux method. For the flux growth, alloy samples of desired compositions were prepared from ingots of aluminium (The Nilaco Corporation, Japan, 99.999 %), ruthenium (Rare Metallic Co., Ltd., Japan, 99.95 %) and silicon (Rare Metallic Co., Ltd., Japan, 99.9999 %) using arc melting in an argon atmosphere (NEV-AD03, Nissin Giken Corporation, Japan). Each sample was then placed in an alumina crucible and sealed in a silica tube in an argon atmosphere. The tube was then heated to 1473 K in a furnace, then cooled at -2 K/h to a desired temperature (1223 K, 1273 K or 1323 K), then kept at the desired temperature for 10 h and then centrifuged, followed by water quenching. Data collection, cell refinement and data reduction were performed using CrysAlis PRO software (Rigaku Oxford Diffraction).[35)] Initial structural models were obtained using SHELXT software,[36)] and subsequent structure refinement was performed using SHELXL software.[37)]

3. Results and Discussion

After investigating several tens of samples, compositional regions of three-phase equilibria in the Al–Ru–Si system near 1200 K were preliminarily determined. Samples that would fall into desired phase equilibria were then prepared to evaluate the composition and unit-cell parameters of each phase involved in each equilibrium. Eight two-phase and 23 three-phase equilibria (from one to three samples for each equilibrium) were investigated. Figure 1 shows the tentative isothermal section of the Al–Ru–Si equilibrium phase diagram near 1200 K drawn on the basis of the data obtained in this study and those adopted from the literature. The nominal compositions of the samples are also shown in Fig. 1. They are basically on the tie lines for two-phase equilibria and inside the tie triangles for three-phase equilibria. For some aluminium-rich samples, they were set at compositions out or on the boundary of the tie triangles to compensate for possible evaporation loss of aluminium (or silicon) during arc melting and annealing. Crystallographic data of the solid phases observed in this study through powder XRD are summarized in Table 1. The composition and unit-cell parameters evaluated for each phase involved in each equilibrium are summarized in Table 2.

3.1 Phase equilibria in the binary systems

Three two-phase equilibria (No. 1–3 in Table 2) were investigated in the binary Al–Ru system, which involve the

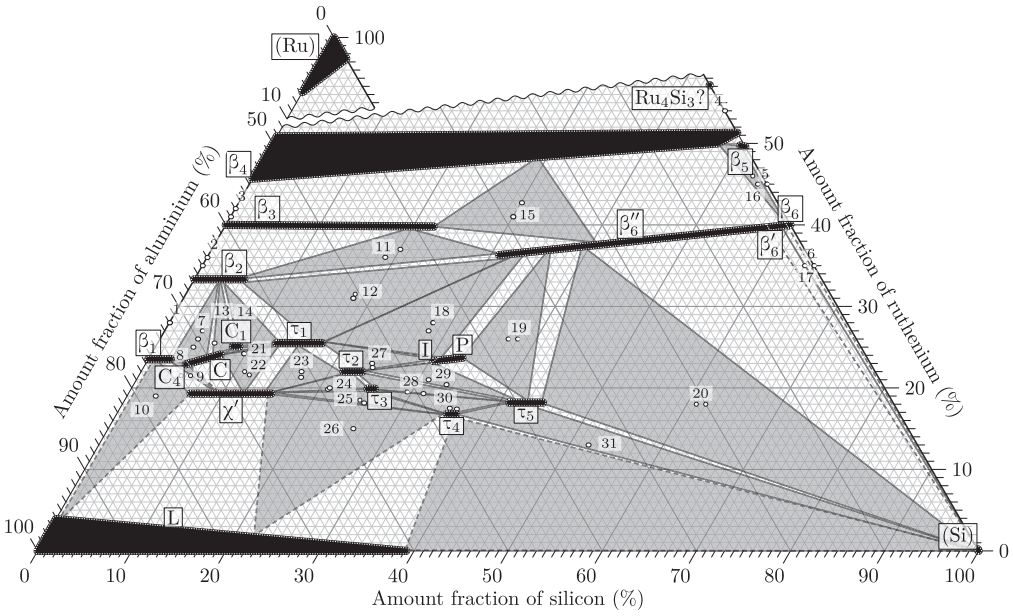

Fig. 1 Tentative isothermal section of the Al–Ru–Si equilibrium phase diagram near 1200 K. Provisional single-phase regions are shown as the black regions with the boundaries shown as the white dotted lines. Tie lines are shown as either solid (confirmed) or dashed (provisional) lines. Three-phase regions are shown as the grey regions (confirmed or provisional in accordance with the surrounding tie lines). The numbers written either inside or near two-phase and three-phase regions correspond to those defined in Table 2. The nominal compositions of the samples are shown as the open circles.

Table 1 Symbols, prototypes (if available), Pearson symbols, (super)space groups of the solid phases in the Al–Ru–Si system observed in this study through powder XRD.

Symbol	Phase	Prototype (Pearson symbol, space group)	References
(Al)	Al	*Cu* (*cF*4, $Fm\bar{3}m$)	38)
(Ru)	Ru	*Mg* (*hP*2, $P6_3/mmc$)	39)
(Si)	Si	*diamond* (*cF*8, $Fd\bar{3}m$)	38)
β_1	Ru_4Al_{13}	Fe_4Al_{13} (*mS*102, $C2/m$)	40)
β_2	$RuAl_2$	$TiSi_2$ (*oF*24, $Fddd$)	8)
β_3	Ru_2Al_3	Os_2Al_3 (*tI*10, $I4/mmm$)	8,41)
β_4	Ru(Al,Si)(*cP*2)	*CsCl* (*cP*2, $Pm\bar{3}m$)	8,10)
β_5	RuSi(*cP*8)	*FeSi* (*cP*8, $P2_13$)	10)
β_6	$Ru_2Si_3(o)$	Ru_2Ge_3 (*oP*40, *Pnca*)	12)
β'_6	$Ru(Al,Si)_\gamma(o)$	Modulated Ru_2Ge_3 [*oP*∗, $Pbma(00\gamma)ss0$][a]	This work
β''_6	$Ru(Al,Si)_\gamma(t)$	$MnSi_\gamma$ [*tI*∗, $I4_1amd(00\gamma)00ss$][a]	This work
C	$\sim Ru_7(Al,Si)_{24}(cP)$	$\sim IrAl_{2.75}$ ($\sim$*cP*31, $Pm\bar{3}$)[b]	This work
C_1	$\sim Ru_7(Al,Si)_{24}(cI)$	$2\times2\times2$ superstructure of C ($\sim$*cI*248, $Im\bar{3}$)[a]	This work
C_4	$\sim Ru_7(Al,Si)_{24}(o)$	$2\times2\times2$ superstructure of C ($\sim$*oS*248, *Ccce*)	This work
χ'	$\sim Ru_{23}(Al,Si)_{97}$	$\sim Fe_{23}(Al,Si)_{97}$ ($\sim$*hP*240, $P6_3/mmc$)	This work
τ_1	$\sim Ru_{16}(Al,Si)_{47}$	No prototype ($\sim$*oS*252, *Cmcm*)	42)
τ_2	$Ru_9(Al,Si)_{32}$	$Fe_9(Al,Si)_{32}$ (*hR*41, $R\bar{3}$)	42)
τ_3	$\sim Ru_{10}(Al,Si)_{41}$	No prototype ($\sim$*oP*204, *Pnma*)	42)
τ_4	$Ru(Al,Si)_5$	$LiIrSn_4$ (*tI*24, $I4/mcm$)	42)
τ_5	$Ru_2(Al,Si)_9$	No prototype (*oS*88, *Cmcm*)	42)
I	$\sim Al_{46}Ru_{23}Si_{31}$	Icosahedral quasicrystal (*iP*∗, $Pm\bar{3}\bar{5}$)[a,c]	This work
P	$\sim Al_{44}Ru_{24}Si_{32}$	2/1 crystalline approximant to I (*cP*∗, $Pm\bar{3}$)[a]	This work

[a] Preliminarily assumed for indexing XRD peaks.
[b] Approximate average structure. Weak $2\times2\times2$ face-centred cubic superstructure reflections were observed in single-crystal XRD.
[c] Nonconventional Pearson symbol *i* stands for *icosahedral*.

Ru_4Al_{13}, $RuAl_2$, Ru_2Al_3 and RuAl(*cP*2) phases (referred to as the β_1, β_2, β_3 and β_4 phases, respectively). According to the recent Al–Ru equilibrium phase diagrams,[43–45] there exist the liquid and Ru phases [referred to as the L and (Ru) phases, respectively] at 1200 K in addition to the above phases. In the samples for the β_2–β_3 equilibrium (No. 2), a

Table 2 Composition and unit-cell parameters (a, b, c, β and $\gamma = c/c'$) of each phase at each equilibrium.

No.	Phase	Composition	a/pm	b/pm	c/pm	β or $\gamma = c/c'$
1	β_1	$Al_{76.3(4)}Ru_{23.7(4)}$	1586.75(14)	819.15(10)	1274.60(8)	107.748(5)°
	β_2	$Al_{66.4(4)}Ru_{33.6(4)}$	801.34(11)	471.82(5)	878.69(11)	—
2[a]	β_2	$Al_{66.7(4)}Ru_{33.3(4)}$	801.26(9)	471.77(6)	878.75(11)	—
	β_3	$Al_{59.9(4)}Ru_{40.1(4)}$	307.99(4)	—	1432.4(2)	—
3	β_3	$Al_{60.2(3)}Ru_{39.8(3)}$	308.01(4)	—	1433.4(2)	—
	β_4	$Al_{54.8(4)}Ru_{45.2(4)}$	299.21(4)	—	—	—
4[a]	(Ru)	$Ru_{97.4(3)}Si_{2.6(3)}$	270.54(6)	—	428.30(18)	—
	β_4	$Ru_{51(2)}Si_{49(2)}$	290.69(3)	—	—	—
5	β_5	$Ru_{49.6(5)}Si_{50.4(5)}$	470.65(5)	—	—	—
	β_6	$Ru_{39.9(5)}Si_{60.1(5)}$	553.40(6)	1105.94(14)	894.96(11)	—
6	β_6	$Ru_{39.9(14)}Si_{60.1(14)}$	553.41(6)	1106.07(13)	895.09(10)	—
	(Si)	$Ru_{0.2(4)}Si_{99.8(4)}$	543.09(7)	—	—	—
7	β_1	$Al_{74.2(11)}Ru_{23.3(10)}Si_{2.4(3)}$	1583.35(13)	819.83(12)	1270.41(11)	107.767(7)°
	β_2	$Al_{64.3(12)}Ru_{33.0(12)}Si_{2.70(14)}$	801.02(12)	470.87(7)	878.39(13)	—
	C	$Al_{70.3(11)}Ru_{23.5(10)}Si_{6.2(3)}$	772.72(10)	—	—	—
8	β_1	—[b]	1583.63(11)	820.01(14)	1271.1(2)	107.766(6)°
	C	$Al_{72.0(4)}Ru_{23.1(4)}Si_{4.87(11)}$	774.47(11)	—	—	—
9	β_1	$Al_{74.5(4)}Ru_{23.5(4)}Si_{2.01(6)}$	1584.19(19)	820.05(10)	1271.12(16)	107.752(3)°
	C_4	$Al_{72.7(4)}Ru_{23.0(4)}Si_{4.29(11)}$	1545.27(17)	1552.9(3)	1549.53(16)	—
	χ'	$Al_{71.1(4)}Ru_{19.2(4)}Si_{9.70(11)}$	1262.84(16)	—	2671.4(3)	—
10	β_1	$Al_{75.7(14)}Ru_{23.7(14)}Si_{0.58(7)}$	1586.1(3)	819.39(10)	1273.57(17)	107.7589(16)°
	χ'	$Al_{74.2(14)}Ru_{19.2(12)}Si_{6.6(5)}$	1265.61(16)	—	2676.0(4)	—
	(Al)[c]	—[d]	404.94(6)	—	—	—
11	β_2	$Al_{62.2(3)}Ru_{33.3(3)}Si_{4.4(3)}$	801.30(12)	470.57(10)	878.16(14)	—
	β_3	$Al_{40.7(4)}Ru_{39.6(3)}Si_{19.69(19)}$	307.14(4)	—	1399.34(19)	—
	β_6''	$Al_{32.7(3)}Ru_{36.5(3)}Si_{30.8(3)}$	573.94(7)	—	457.73(6)	1.7234(2)
12	β_2	$Al_{61.8(6)}Ru_{32.9(4)}Si_{5.3(8)}$	801.04(12)	470.25(8)	878.37(13)	—
	β_6''	$Al_{32.1(3)}Ru_{35.9(3)}Si_{32.0(4)}$	573.62(7)	—	457.50(6)	1.7194(3)
	τ_1	$Al_{57.7(6)}Ru_{25.2(4)}Si_{17.1(8)}$	762.91(11)	2344.6(3)	2067.3(3)	—
13	β_2	$Al_{63.9(8)}Ru_{33.4(8)}Si_{2.69(16)}$	801.13(10)	470.87(6)	878.58(11)	—
	C	$Al_{69.4(7)}Ru_{24.1(6)}Si_{6.6(3)}$	772.21(8)	—	—	—
	C_1	$Al_{66.7(7)}Ru_{25.0(6)}Si_{8.4(3)}$	1541.55(15)	—	—	—
14	β_2	$Al_{63.7(6)}Ru_{32.9(6)}Si_{3.34(12)}$	800.97(12)	470.63(8)	878.37(13)	—
	C_1	$Al_{66.0(5)}Ru_{25.2(4)}Si_{8.8(3)}$	1540.81(19)	—	—	—
	τ_1	$Al_{61.5(5)}Ru_{25.5(4)}Si_{13.0(3)}$	769.21(12)	2351.5(3)	2066.5(3)	—
15	β_3	$Al_{38.0(8)}Ru_{39.8(7)}Si_{22.2(7)}$	307.54(5)	—	1393.94(17)	—
	β_4	$Al_{22.7(12)}Ru_{48.3(9)}Si_{29.0(8)}$	293.74(4)	—	—	—
	β_6''	$Al_{21.7(8)}Ru_{37.9(7)}Si_{40.4(7)}$	567.69(7)	—	451.01(6)	1.64546(13)
16	β_4	$Al_{2.7(3)}Ru_{49.9(4)}Si_{47.4(4)}$	292.08(4)	—	—	—
	β_5	$Al_{0.45(7)}Ru_{49.7(3)}Si_{49.8(3)}$	470.69(6)	—	—	—
	β_6' or β_6	$Al_{0.4(3)}Ru_{39.9(4)}Si_{59.7(4)}$	553.42(5)	1106.08(13)	447.45(12)	1.4997(4)
17	β_6'	$Al_{1.04(6)}Ru_{39.6(4)}Si_{59.4(4)}$	554.34(7)	1108.07(14)	447.32(5)	1.5086(3)
	(Si)	$Al_{0.00(5)}Ru_{0.000(14)}Si_{100.00(5)}$	543.04(9)	—	—	—
18	β_6''	$Al_{29.4(6)}Ru_{37.0(5)}Si_{33.6(5)}$	572.01(6)	—	456.00(6)	1.7010(3)
	τ_1	$Al_{56.8(7)}Ru_{25.7(5)}Si_{17.6(4)}$	761.93(12)	2340.8(4)	2066.1(3)	—
	P	$Al_{45.2(7)}Ru_{23.7(5)}Si_{31.1(4)}$[f]	1938.5(3)	—	—	—
	I[e]		435.74(8)	—	—	—
19	β_6''	$Al_{26.7(4)}Ru_{37.4(3)}Si_{35.9(3)}$	570.58(7)	—	454.35(6)	1.68156(10)
	τ_5	$Al_{38.7(5)}Ru_{18.4(3)}Si_{42.9(3)}$	864.85(12)	879.61(10)	1745.4(3)	—
	P	$Al_{43.0(5)}Ru_{23.8(3)}Si_{33.2(3)}$	1935.2(3)	—	—	—
20	β_6''	$Al_{23.4(5)}Ru_{37.5(5)}Si_{39.1(6)}$	569.09(8)	—	452.50(7)	1.66050(10)
	τ_5	$Al_{37.4(7)}Ru_{18.2(3)}Si_{44.5(6)}$	862.47(5)	878.78(12)	1747.0(3)	—
	(Si)	$Al_{0.1(7)}Ru_{0.0(3)}Si_{99.9(6)}$	543.20(7)	—	—	—
21	C	$Al_{68.8(5)}Ru_{24.0(4)}Si_{7.22(17)}$	771.81(7)	—	—	—
	C_1	$Al_{66.2(5)}Ru_{25.0(4)}Si_{8.81(17)}$	1541.33(17)	—	—	—
	τ_1	$Al_{62.1(5)}Ru_{25.1(4)}Si_{12.7(3)}$	770.24(9)	2352.3(3)	2066.5(3)	—
22	C	$Al_{68.4(6)}Ru_{24.1(5)}Si_{7.45(18)}$	771.66(10)	—	—	—
	χ'	$Al_{68.5(6)}Ru_{19.3(5)}Si_{12.22(18)}$	1260.36(15)	—	2667.2(4)	—
	τ_1	$Al_{61.4(6)}Ru_{25.5(4)}Si_{13.1(4)}$	768.83(11)	2352.0(4)	2066.4(3)	—
23	χ'	$Al_{66.4(12)}Ru_{19.2(8)}Si_{14.4(8)}$	1257.66(13)	—	2663.6(5)	—
	τ_1	$Al_{59.7(12)}Ru_{25.2(9)}Si_{15.1(6)}$	764.80(11)	2347.6(4)	2068.2(3)	—
	τ_2	$Al_{56.6(12)}Ru_{21.7(8)}Si_{21.7(8)}$	1045.34(15)	—	1968.6(3)	—
24	χ'	$Al_{65.5(3)}Ru_{19.46(19)}Si_{15.1(3)}$	1256.02(17)	—	2661.4(6)	—
	τ_2	$Al_{55.7(3)}Ru_{21.9(2)}Si_{22.4(3)}$	1044.81(14)	—	1967.2(3)	—
	τ_3	$Al_{54.9(3)}Ru_{19.88(19)}Si_{25.2(3)}$	1508.5(2)	1187.91(13)	1695.3(3)	—
25	χ'	$Al_{65.4(4)}Ru_{19.4(2)}Si_{15.2(4)}$	1256.90(8)	—	2659.12(18)	—
	τ_3	$Al_{55.0(4)}Ru_{19.6(2)}Si_{25.4(4)}$	1508.68(19)	1188.27(13)	1695.7(3)	—
	τ_4	$Al_{48.1(4)}Ru_{16.7(2)}Si_{35.2(4)}$	620.51(9)	—	968.42(14)	—
26	χ'	$Al_{65.9(16)}Ru_{19.3(11)}Si_{14.8(10)}$	1258.72(18)	—	2666.7(4)	—
	τ_4	$Al_{48.6(19)}Ru_{16.8(10)}Si_{34.6(17)}$	620.96(8)	—	967.82(11)	—
	(Al)[c]	—[d]	404.96(6)	—	—	—
	(Si)[c]	—[d]	543.16(6)	—	—	—
27	τ_1	$Al_{57.1(7)}Ru_{25.7(6)}Si_{17.2(5)}$	762.42(12)	2342.4(4)	2067.5(3)	—
	τ_2	$Al_{54.5(8)}Ru_{22.1(5)}Si_{23.4(7)}$	1044.59(13)	—	1964.5(3)	—
	I	$Al_{46.0(8)}Ru_{23.5(5)}Si_{30.5(7)}$	435.85(6)	—	—	—
28	τ_2	$Al_{55.2(12)}Ru_{22.0(8)}Si_{22.8(9)}$	1044.61(14)	—	1965.5(3)	—
	τ_3	$Al_{54.1(12)}Ru_{19.8(7)}Si_{26.1(10)}$	1508.0(2)	1187.16(16)	1693.19(17)	—
	τ_5	$Al_{40.7(12)}Ru_{18.3(7)}Si_{41.0(10)}$	867.01(9)	881.54(13)	1742.7(4)	—
29	τ_2	$Al_{54.2(8)}Ru_{22.1(5)}Si_{23.7(6)}$	1044.27(13)	—	1963.6(3)	—
	τ_5	$Al_{39.6(8)}Ru_{18.4(5)}Si_{42.0(6)}$	866.27(12)	880.78(11)	1743.2(2)	—
	P	$Al_{46.4(8)}Ru_{23.1(5)}Si_{30.5(7)}$[f]	1939.2(3)	—	—	—
	I[e]		435.88(6)	—	—	—
30	τ_3	$Al_{54.9(12)}Ru_{19.8(7)}Si_{25.3(9)}$	1508.19(17)	1187.31(16)	1694.9(2)	—
	τ_4	$Al_{48.0(12)}Ru_{16.8(6)}Si_{35.2(12)}$	619.96(9)	—	968.38(10)	—
	τ_5	$Al_{40.8(12)}Ru_{18.3(6)}Si_{40.9(12)}$	866.91(10)	881.98(13)	1741.1(3)	—
31	τ_4	$Al_{47.1(4)}Ru_{16.8(2)}Si_{36.1(4)}$	619.64(7)	—	969.17(13)	—
	τ_5	$Al_{40.0(4)}Ru_{18.4(3)}Si_{41.7(4)}$	866.72(11)	882.15(10)	1741.9(3)	—
	(Si)	$Al_{0.2(4)}Ru_{0.0(2)}Si_{99.8(4)}$	543.14(7)	—	—	—

Continued on next column.

Continued.

[a] Not fully in equilibrium.
[b] Analysable grains could not be found in SEM.
[c] Probably crystallized from the L phase during cooling.
[d] Not determined.
[e] Probably transformed from the P phase during cooling.
[f] The P and I phases could not be distinguished in SEM.

minor β_4 phase was observed in powder XRD and SEM, which may have primarily crystallized from melt during solidification and remained even after a long-time annealing. The existence of the primary β_4 phase indicates that these samples are inhomogeneous and not fully in equilibrium, and the homogeneity could not be improved even after sintering processes. The compositions of the β_2 and β_3 phases were analysed at regions far from the β_4 phase in these samples. The compositions of the β_1, β_2 and β_3 phases are consistent with their stoichiometry and those reported in the recent phase diagrams.[43–45] The composition of the β_4 phase at the β_3–β_4 equilibrium (No. 3) is consistent with that given in Gobran *et al.*[44] The composition of the β_4 phase at the β_4–(Ru) equilibrium (not investigated in this study) was therefore adopted from Gobran *et al.*[44] in drawing Fig. 1. The other compositions [L at L–β_1 and (Ru) at β_4–(Ru)] were adopted from Liu *et al.*[45]

Three two-phase equilibria (No. 4–6 in Table 2) were investigated in the binary Ru–Si system, which involve the Ru, RuSi(*cP*2), RuSi(*cP*8), Ru_2Si_3(*o*) and Si phases [referred to as the (Ru), β_4, β_5, β_6 and (Si) phases, respectively]. The phase equilibria and the associated compositions in the Ru–Si system are essentially consistent with those reported by Perring *et al.*[46] although the reported compositions are systematically deficient in silicon. They attributed this deficiency to the PAP model,[47] which they used for the matrix correction. Table 3 shows the compositions of the stoichiometric phases in the Al–Ru and Ru–Si systems (β_1, β_2, β_3, β_5 and β_6) evaluated using different matrix correction models. While the compositions evaluated using the PAP model are systematically deficient in aluminium or silicon, those evaluated using the Armstrong/Love–Scott model (adopted in this study) are consistent with the stoichiometry. The reason why the Armstrong/Love–Scott model gives better compositions for these phases than the PAP model is under investigation.

In the sample for the (Ru)–β_4 equilibrium (No. 4), a minor phase with the composition $Ru_{57(2)}Si_{43(2)}$ was observed only in SEM; thus, this sample is not fully in equilibrium. The minor phase may be identified as the Ru_4Si_3 phase from the composition. According to Perring *et al.*,[46] existence of the Ru_4Si_3 phase below 1473 K is questionable. Possible existence of the Ru_4Si_3 phase near 1200 K is indicated in Fig. 1 by "Ru_4Si_3?". Note that Liu *et al.*[48] and Du *et al.*[49] also reported phase diagrams of the Ru–Si system, and the Ru_4Si_3 phase exists at 1200 K as an equilibrium phase in their phase diagrams. However, their phase diagrams were derived in terms of thermodynamic assessment of available experimental data, mainly those given by Perring *et al.*;[46]

Table 3 Compositions of the stoichiometric phases in the Al–Ru and Ru–Si systems evaluated using different matrix correction models.

Phase	Stoichiometry	Armstrong/Love–Scott	PAP (This work)	PAP (Perring *et al.*[46])
β_1 (No. 1)	Ru_4Al_{13}	$Ru_4Al_{12.8(3)}$	$Ru_4Al_{12.2(3)}$	—
β_2 (No. 1)	$RuAl_2$	$RuAl_{1.97(3)}$	$RuAl_{1.86(3)}$	—
β_2 (No. 2)	$RuAl_2$	$RuAl_{2.01(3)}$	$RuAl_{1.89(3)}$	—
β_3 (No. 2)	Ru_2Al_3	$Ru_2Al_{2.99(5)}$	$Ru_2Al_{2.80(5)}$	—
β_3 (No. 3)	Ru_2Al_3	$Ru_2Al_{3.03(4)}$	$Ru_2Al_{2.83(4)}$	—
β_5 (No. 5)	RuSi	$RuSi_{1.017(19)}$	$RuSi_{0.965(18)}$	$RuSi_{0.97}$
β_6 (No. 5)	Ru_2Si_3	$Ru_2Si_{3.02(6)}$	$Ru_2Si_{2.88(6)}$	$Ru_2Si_{2.88}$
β_6 (No. 6)	Ru_2Si_3	$Ru_2Si_{3.01(17)}$	$Ru_2Si_{2.87(17)}$	$Ru_2Si_{2.89}$

thus, the existence of the Ru_4Si_3 phase at 1200 K in their phase diagrams has not been justified experimentally. Solution of silicon in the (Ru) phase of 2.6(3) % was observed in this sample. By comparing this to the solubility data given by Perring *et al.*,[46] the actual annealing temperature may be estimated to be near 1473 K. However, this much higher temperature than 1200 K is unrealistic considering our experimental set-up. Instead, it may be another evidence that this sample is not fully in equilibrium. The $RuSi_2$ phase reported by Ivanenko *et al.*[50] was not observed in this study. Note that occurrence of the two RuSi phases (β_4 and β_5) at different compositions, which is consistent with Perring *et al.*'s observation,[46] is not reflected in the recent thermodynamic assessments[48,49] and compilation[51] of the Ru–Si system.

No phase equilibria were investigated in the binary Al–Si system. According to Murray and McAlister,[52] there exist only the L and (Si) phases at 1200 K. Compositions adopted from Murray and McAlister[52] were used in drawing Fig. 1.

3.2 Ternary solid solutions in the binary phases

Solution of silicon in the Al–Ru binary phases (β_1, β_2, β_3 and β_4) were observed in ten equilibria (No. 7–16 in Table 2). From the compositions, these solutions seem to be substitutional (silicon for aluminium) with small variation in the ruthenium fraction for the β_4 phase. The solubility limits of silicon in the β_1, β_2 and β_3 phases are approximately 2 %, 5 % and 22 %, respectively. The β_4 phase seems to be a complete solid solution between RuAl(*cP*2) and RuSi(*cP*2). The unit-cell lengths in these phases basically decrease with increasing silicon fraction (see Table 2). An obvious exception is the length b in the β_1 phase, which roughly increases with increasing silicon fraction. Solution of aluminium in the β_5 phase was observed in one equilibrium (No. 16 in Table 2) with a low solubility limit of approximately 0.5 %.

An extension of the β_6 phase (referred to as β_6' or β_6'' depending on the composition) in the Al–Ru–Si system was observed in eight equilibria (No. 11, 12, 15–20 in Table 2). The crystal structure of the β_6 phase is of the Ru_2Ge_3 type (see Table 1), and the Ru_2Ge_3 type with the space-group setting *Pnca* is a $1 \times 2 \times 1$ superstructure of the Ru_2Sn_3 type.[53] For the β_6 phase, an XRD peak indexed as *hkl* with $k = 2n + 1$ (n is an integer) corresponds to a superstructure reflection. Figure 2 shows powder XRD patterns taken from samples at the β_6–(Si), β_6'–(Si) and β_3–β_4–β_6'' equilibria

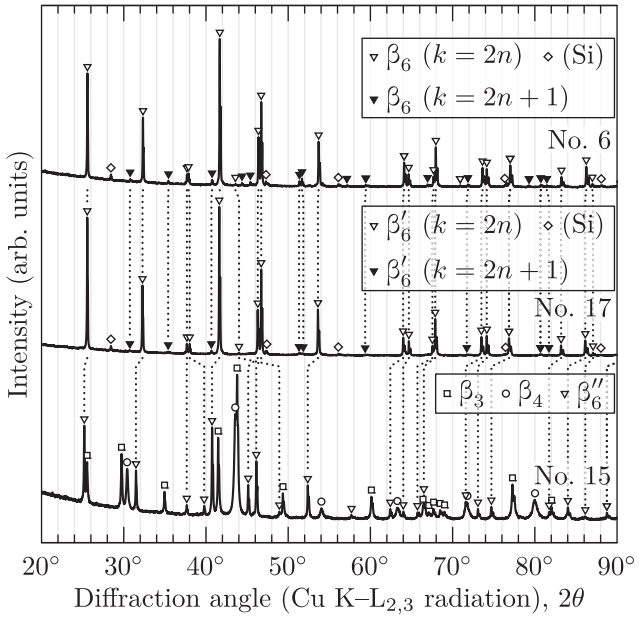

Fig. 2 Powder XRD patterns taken from samples at the β_6–(Si), β_6'–(Si) and β_3–β_4–β_6'' equilibria (No. 6, 17 and 15, respectively, in Table 2).

(No. 6, 17 and 15, respectively). The aluminium fraction in the β_6, β_6' and β_6'' phases increases in this order. While superstructure reflections were observed for the β_6 and β_6' phases, no such reflections were observed for the β_6'' phase. Most of the peaks due to the β_6' and β_6'' phases shift toward lower angles compared to the β_6 phase, which can be attributed to increase in the unit-cell lengths (in terms of the basic Ru_2Sn_3-type structure) with increasing aluminium fraction. Some peaks, however, shift toward higher angles, and another length parameter is required to account for this behaviour.

Powder XRD peaks from the β_6'' phase can be indexed assuming the $MnSi_\gamma$ type[20] (see Table 1). The $MnSi_\gamma$ phase ($\gamma \approx 1.74$) is an NCL phase with an incommensurate composite-crystalline structure characterized by two lengths along the c axis, c for the [Mn] subsystem and c' for the [Si] subsystem, and $\gamma = c/c'$ is the ratio of the two lengths. The $MnSi_\gamma$ type can be regarded as an incommensurately modulated variant of the Ru_2Sn_3 type. In a similar way, powder XRD peaks from the β_6' phase can be indexed assuming a superstructure of the $MnSi_\gamma$ type (or an incommensurately modulated variant of the Ru_2Ge_3 type) (see Table 1). The space group $P\bar{4}c2$ of the Ru_2Sn_3 type can

be deduced from the superspace group $I4_1/amd(00\gamma)00ss$ of the $MnSi_\gamma$ type with $\gamma = 3/2$ (i.e. commensurate case).[54] The superspace group $Pbma(00\gamma)ss0$ was chosen for the β_6' phase so that a similar relation holds with the Ru_2Ge_3 type.

The combined composition range of the β_6, β_6' and β_6'' phases is approximately from $Al_{33}Ru_{36}Si_{31}$ [$Ru(Al_{0.51}Si_{0.49})_{1.7}$] to $Ru_{67}Si_{33}$ ($RuSi_{1.5}$), which may contain the compositions $Ru(Al_{0.2}Si_{0.8})_{2-x}$ and $Ru(Al_{0.5}Si_{0.5})_{2-x}$ mentioned by Nowotny and coworkers[14–16] although it cannot be confirmed as the value of x is not reported. The reason why Nowotny and coworkers could not determine the unit-cell parameters of $Ru(Al_{0.2}Si_{0.8})_{2-x}$ and $Ru(Al_{0.5}Si_{0.5})_{2-x}$ might be that they are incommensurate composite crystals, which were probably not common at that time. The phase boundaries between the β_6, β_6' and β_6'' phases are not clear from our data. The unit-cell lengths in these phases basically increase with increasing aluminium fraction except for c', which decreases with increasing aluminium fraction (see Table 2).

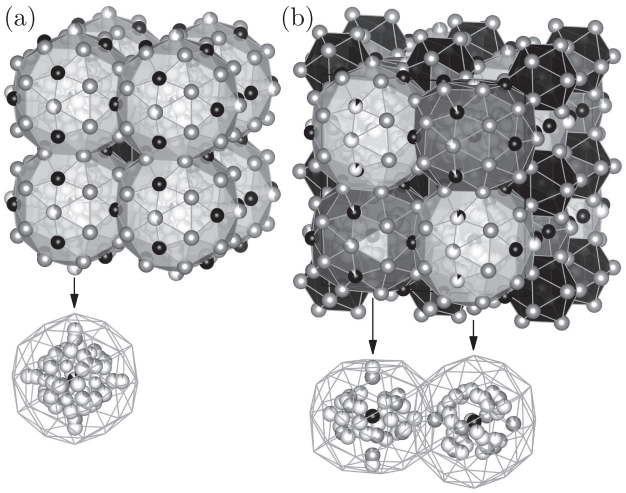

Fig. 3 Crystal structures of the (a) C and (b) C_4 phases visualized using VESTA 3 software.[59] Colour codes: grey spheres for aluminium and silicon, black spheres for ruthenium, black polyhedra for icosahedral clusters and white and grey polyhedra for pseudo-Mackay clusters.

3.3 C and related phases

The C phase was observed in five equilibria (No. 7, 8, 13, 21 and 22 in Table 2). The homogeneity range of the C phase was found to be approximately from $Al_{72}Ru_{23}Si_5$ to $Al_{69}Ru_{24}Si_7$. Near the composition of the C phase, two new phases (referred to as the C_1 and C_4 phases) were discovered (see Fig. 1). The C_1 phase was observed in three equilibria (No. 13, 14 and 21) near the composition $Al_{66}Ru_{25}Si_9$, and the C_4 phase was observed in one equilibrium (No. 9) near the composition $Al_{73}Ru_{23}Si_4$.

Single crystals of the C and C_4 phases could be grown using the self-flux method from alloy samples with the nominal compositions $Al_{66.5}Ru_{10.0}Si_{23.5}$ and $Al_{79.0}Ru_{10.0}Si_{11.0}$, respectively. Crystal data, data collection and structure refinement details are summarized in the Crystallographic Information File (CIF) format and available online.[55] For the C phase, weak $2 \times 2 \times 2$ face-centred cubic superstructure reflections were observed in single-crystal XRD, but only an approximate average structure could be solved as a $1 \times 1 \times 1$ simple cubic basic structure as shown in Fig. 3(a). The structure can be viewed as a *CsCl*-type packing of icosahedral and so-called pseudo-Mackay clusters, and the inner-shell structure of the pseudo-Mackay cluster is highly disordered similarly to the other known structures of the C phases in other systems.[56–58] Note that no significant XRD peaks corresponding to the superstructure reflections are found in the powder XRD patterns probably because of the weak intensities, and the Le Bail analyses could be done assuming the basic structure without difficulty. The structure of the C_4 phase was found to be a $2 \times 2 \times 2$ side-face-centred orthorhombic superstructure of the C phase as shown in Fig. 3(b). Two types of pseudo-Mackay clusters with different inner-shell configurations constitute the superstructure ordering. Distinction between aluminium and silicon is rather ambiguous from the structure refinement for these two phases, particularly at partially occupied sites.

Superstructures of the C phase (not necessarily in the Al–Ru–Si system) had been found in three forms, $2 \times 2 \times 2$ body-centred cubic, $2 \times 2 \times 2$ face-centred cubic and $\sqrt{2} \times \sqrt{2} \times \sqrt{3}$ hexagonal, and they are referred to as the C_1, C_2 and C_3 phases, respectively, in the nomenclature of Grushko and Velikanova.[6] The name C_4 was chosen because it is the fourth form of the superstructures of the C phase. Powder XRD peaks from the C_1 phase can be indexed assuming a $2 \times 2 \times 2$ body-centred cubic superstructure of the C phase, and that is why this phase is referred to as the C_1 phase. The unit-cell lengths in the C, C_1 and C_4 phases (in terms of the basic structure of the C phase and on average over a, b and c for the C_4 phase) decrease with increasing silicon fraction.

3.4 Other ternary phases

The χ' phase was observed in seven equilibria (No. 9, 10, 22–26 in Table 2). The homogeneity range of the χ' phase was found to be approximately from $Al_{74}Ru_{19}Si_7$ to $Al_{66}Ru_{19}Si_{15}$, which is 2 % wider on the silicon-rich side than that deduced from the compositions of single crystals reported by Morrison *et al.*[28] The unit-cell lengths basically decrease with increasing silicon fraction as is mentioned in Morrison *et al.*[28] A large single crystal of the χ' phase was obtained as a by-product of growing single crystals of the C phase using the self-flux method from an alloy sample with the nominal composition $Al_{74.0}Ru_{10.0}Si_{16.0}$. Crystal data, data collection and structure refinement details are summarized in the CIF format and available online.[60] The structure of the χ' phase determined in this study is quite similar to that of $Ru_{23}(Al,Si)_{97}$ reported by Morrison *et al.*,[28] but there are some remarkable differences. First of all, the positions of some atoms given in Table 1 in Morrison *et al.*[28] are inconsistent with the structure shown in their Fig. 2 probably because of severe typos. They stated that the structure of $Ru_{23}(Al,Si)_{97}$ is similar to that of $\sim Fe_{23}(Al,Si)_{97}$[61,62] with the difference being that there are neither positionally disordered nor partially occupied sites in $Ru_{23}(Al,Si)_{97}$. In this study, however, positionally disordered and partially occupied sites as seen in $\sim Fe_{23}(Al,Si)_{97}$ were deduced from the structure refinement, and thus the formula $\sim Ru_{23}(Al,Si)_{97}$ should be more suitable than $Ru_{23}(Al,Si)_{97}$ for the χ' phase. In addition, aluminium and silicon could be distinguished to some extent

from the structure refinement in this study, while the distinction was completely ignored in Morrison *et al.*[28]

Five new crystalline phases (referred to as the τ_1, τ_2, τ_3, τ_4 and τ_5 phases) were observed in 16 equilibria (No. 12, 14, 18–31 in Table 2) and identified as follows. Small single crystals of these phases could be obtained from nearly single-phase samples. Results of the single-crystal XRD analyses were reported elsewhere.[42] Powder XRD peaks from these phases can be indexed assuming the structures deduced from the single-crystal XRD analyses (see Table 1). The homogeneity ranges of these phases are approximately from $Al_{62}Ru_{25}Si_{13}$ to $Al_{56}Ru_{26}Si_{18}$ for τ_1, from $Al_{57}Ru_{22}Si_{21}$ to $Al_{54}Ru_{22}Si_{24}$ for τ_2, from $Al_{55}Ru_{20}Si_{25}$ to $Al_{54}Ru_{20}Si_{26}$ for τ_3, from $Al_{49}Ru_{17}Si_{34}$ to $Al_{47}Ru_{17}Si_{36}$ for τ_4 and from $Al_{41}Ru_{18}Si_{41}$ to $Al_{37}Ru_{18}Si_{45}$ for τ_5. The unit-cell lengths in these phases basically decrease with increasing silicon fraction. Obvious exceptions are the length c in the τ_4 and τ_5 phases, which roughly increase with increasing silicon fraction.

The other two new phases (referred to as the I and P phases) were observed in four equilibria (No. 18, 19, 27 and 29 in Table 2) and identified as follows. The I phase was first identified as an icosahedral quasicrystal employing an automated identification system based on machine learning at an early stage of this study. The details of the identification will be reported elsewhere.[63] A rather systematic way of identification of the I phase employing the Le Bail method is shown here. Figure 4(a) shows results of the Le Bail analysis for a sample of the τ_1–τ_2–I equilibrium (No. 27) with only the τ_1 and τ_2 phases taken into account. It was found that significant peaks in the absolute residual can be indexed assuming a primitive icosahedral quasicrystal (the indexing scheme of Elser[64] is used in this study). Le Bail analysis was then performed taking into account the icosahedral quasicrystal. The icosahedral quasicrystal was treated as a six-dimensional modulated structure in the Jana2006 software with only twelve typically strong reflections taken into account. Note that this phase was identified as a face-centred icosahedral quasicrystal via electron diffraction,[63] but no significant XRD peaks corresponding to face-centred superstructure reflections are found in the powder XRD patterns probably because of very weak intensities in XRD. A primitive icosahedral quasicrystal is therefore assumed to simplify the indexing and Le Bail analysis. Results of the Le Bail analysis are shown in Fig. 4(b), and no significant peaks are found in the absolute residual in this case. In a similar way, the P phase was identified as a cubic 2/1 rational crystalline approximant[24] to the I phase from the Le Bail analysis for a sample of the β_6''–τ_5–P equilibrium (No. 19). Samples with the other two conditions (No. 18 and 29) consist of four phases including both I and P. In our preliminary annealing experiments at 1000 K, the P phase has never been observed. Probably, the above samples were in equilibrium near 1200 K without the I phase, but a part of the P phase transformed into the I phase during cooling. The combined composition range of the I and P phases is approximately from $Al_{46}Ru_{23}Si_{31}$ to $Al_{43}Ru_{24}Si_{33}$. On the basis of the above results and discussion, we tentatively assigned the aluminium-rich and silicon-rich sides to the I and P phases, respectively. However, equilibrium involving these two phases should be investigated in more detail, taking into account temperature dependence. The unit-cell lengths in these phases decrease with increasing silicon fraction.

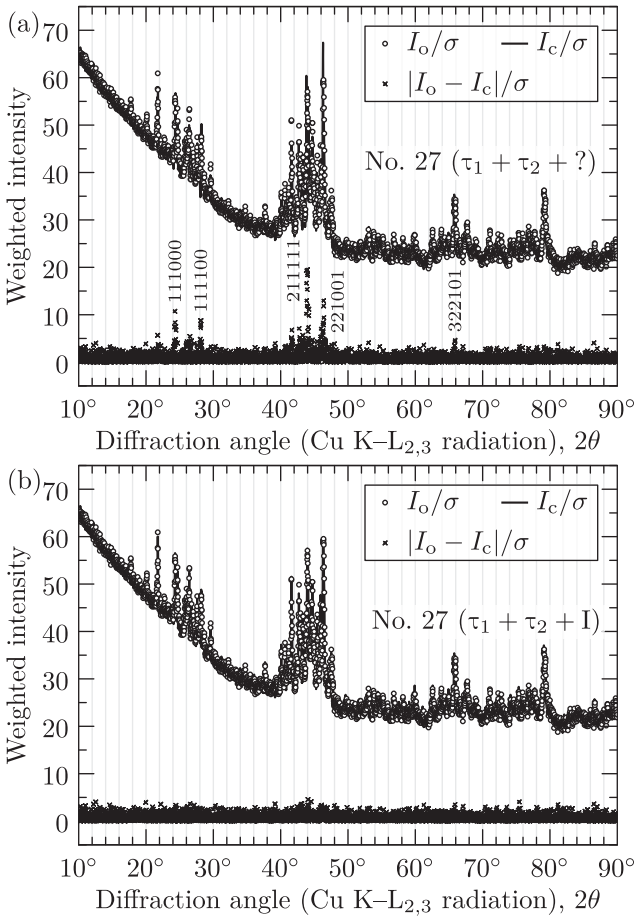

Fig. 4 (a) Results of the Le Bail analysis for a sample of the τ_1–τ_2–I equilibrium (No. 27 in Table 2) with only the τ_1 and τ_2 phases taken into account. I_o and I_c are the observed and calculated intensities, respectively. σ is the standard deviation of I_o and was estimated to be equal to $\sqrt{I_o}$. (b) Similar to (a) but with the I phase taken into account.

It was found unlikely to achieve equilibrium in the ruthenium-rich region (the amount fraction of ruthenium higher than 50 %) near 1200 K within a reasonable time. As far as investigated (up to approximately 2000 h), only the (Ru) and β_4 phases (and possibly the Ru_4Si_3 phase, see Sec. 3.1) were observed in the ruthenium-rich region. Therefore no other phases are expected in this region.

4. Conclusion

Phase equilibria in the Al–Ru–Si system near 1200 K were thoroughly investigated through prolonged-annealing experiments. The composition and unit-cell parameters of each phase involved in each equilibrium were evaluated at eight two-phase and 23 three-phase equilibria, and a tentative isothermal section of the Al–Ru–Si equilibrium phase diagram near 1200 K was drawn on the basis of those data and the data adopted from the literature. In the course of the investigation, eleven new ternary phases including two incommensurate composite-crystalline (β_6' and β_6'') and an icosahedral quasicrystalline (I) phases were identified. In addition, single crystals of some ternary phases could be

obtained, and their crystal structures were determined using single-crystal XRD.

Note that the existence of the quasicrystalline (I) phase in the Al–Ru–Si system was not predicted by the recently developed machine-learning model for predicting compositions of quasicrystals,[65] which was trained using known compositions of known quasicrystals and successfully used for discovering three new quasicrystals.[66] This may indicate that the I phase in the Al–Ru–Si system has somewhat different characteristics from previously known quasicrystals, by which the machine-learning model could not predict the existence from the training data. Two obvious differences are the amount fraction of aluminium of approximately 46 % and unit-cell parameter of approximately 435.8 pm (see Table 2), which are from 65 % to 72 % and from 446.5 pm to 461.7 pm, respectively, for previously known stable icosahedral quasicrystals composed of aluminium and late transition elements.[67]

As a final remark, single-phase boundaries drawn in Fig. 1 should be considered provisional. These boundaries were drawn with straight line segments so that the compositions at the investigated equilibria and those adopted from the literature are reasonably covered by the single-phase regions. However, segments of the boundaries are not necessarily straight, i.e. they are curved in general. In contrast, there is no such ambiguity in the three-phase regions. In any case, the phase diagram shown in Fig. 1 should be a good starting point for further investigations in the Al–Ru–Si system.

Acknowledgements

Most of the sample preparations, powder XRD measurements and SEM–EDS measurements were performed with the help of Ms Itaya and Ms Nakamura at The University of Tokyo. Single-crystal growth using the self-flux method and preliminary single-crystal XRD analyses for the C, C_4 and χ' phases were performed with the help of Mr Shibata at Hokkaido University. This work was supported by JSPS KAKENHI Grant number JP19H05818, JP19H05819 and JP19K15274.

REFERENCES

1) G.J. Snyder and E.S. Toberer: Nat. Mater. **7** (2008) 105–114.
2) X. Zhang and L.-D. Zhao: J. Materiomics **1** (2015) 92–105.
3) W. Liu, J. Hu, S. Zhang, M. Deng, C.-G. Han and Y. Liu: Mater. Today Phys. **1** (2017) 50–60.
4) Y. Shiota, H. Muta, K. Yamamoto, Y. Ohishi, K. Kurosaki and S. Yamanaka: Intermetallics **89** (2017) 51–56.
5) Y. Iwasaki, K. Kitahara and K. Kimura: Phys. Rev. Mater. **3** (2019) 061601(R).
6) B. Grushko and T. Velikanova: Calphad **31** (2007) 217–232.
7) Y. Iwasaki, K. Kitahara and K. Kimura: Phys. Rev. Mater. **5** (2021) 125401.
8) L.-E. Edshammar: Acta Chem. Scand. **20** (1966) 427–431.
9) D. Mandrus, V. Keppens, B.C. Sales and J.L. Sarrao: Phys. Rev. B **58** (1998) 3712–3716.
10) K. Göransson, I. Engström and B. Noläng: J. Alloy. Compd. **219** (1995) 107–110.
11) H. Hohl, A.P. Ramirez, C. Goldmann, G. Ernst and E. Bucher: J. Alloy. Compd. **278** (1998) 39–43.
12) P. Israiloff and H. Völlenkle: Monatsh. Chem. **105** (1974) 1313–1321.
13) C.P. Susz, J. Muller, K. Yvon and E. Parthé: J. Less-Common Met. **71** (1980) P1–P8.
14) O. Schwomma, A. Preisinger, H. Nowotny and A. Wittmann: Monatsh. Chem. **95** (1964) 1527–1537.
15) A. Wittmann and H. Nowotny: J. Less-Common Met. **9** (1965) 303–304.
16) H. Völlenkle, A. Preisinger, H. Nowotny and A. Wittmann: Z. Kristallogr. **124** (1967) 9–25.
17) W.B. Pearson: Acta Crystallogr. Sec. B **26** (1970) 1044–1046.
18) I. Nishida: J. Mater. Sci. **7** (1972) 435–440.
19) N. Sato, H. Ouchi, Y. Takagiwa and K. Kimura: Chem. Mater. **28** (2016) 529–533.
20) Y. Miyazaki, D. Igarashi, K. Hayashi, T. Kajitani and K. Yubuta: Phys. Rev. B **78** (2008) 214104.
21) W. Li, Y. Li, X. Ma and Z. Zhang: Mater. Chem. Phys. **148** (2014) 490–493.
22) Y. Miyazaki, T. Nakajo, Y. Kikuchi and K. Hayashi: J. Mater. Res. **30** (2015) 2611–2617.
23) N. Koshikawa, M. Ohtsuki, K. Edagawa, S. Yoda, R. Tamura and S. Takeuchi: J. Alloy. Compd. **342** (2002) 35–37.
24) K. Niizeki: J. Phys. A **25** (1992) 1843–1854.
25) T. Takeuchi, T. Otagiri, H. Sakagami, T. Kondo, U. Mizutani and H. Sato: Phys. Rev. B **70** (2004) 144202.
26) Y. Takagiwa, T. Kamimura, S. Hosoi, J.T. Okada and K. Kimura: Z. Kristallogr. **224** (2009) 21–25.
27) Y. Takagiwa and K. Kimura: Sci. Technol. Adv. Mater. **15** (2014) 044802.
28) G.W. Morrison, M.C. Menard, L.J. Treadwell, N. Haldolaarachchige, K.C. Kendrick, D.P. Young and J.Y. Chan: Philos. Mag. **92** (2012) 2524–2540.
29) S. Katrych, V. Gramlich and W. Steurer: J. Alloy. Compd. **407** (2006) 132–140.
30) J.T. Armstrong: *Electron Probe Quantitation*, ed. by K.F.J. Heinrich and D.E. Newbury, (Springer, Boston, MA, 1991) pp. 261–315. doi:10.1007/978-1-4899-2617-3_15
31) V.D. Scott and G. Love: *Electron Probe Quantitation*, ed. by K.F.J. Heinrich and D.E. Newbury, (Springer, Boston, MA, 1991) pp. 19–30. doi:10.1007/978-1-4899-2617-3_3
32) T. Kato, M.-J. Jeen and D.-L. Cho: J. Earth Planet. Sci. Nagoya Univ. **60** (2013) 93–100.
33) A. Le Bail, H. Duroy and J.L. Fourquet: Mater. Res. Bull. **23** (1988) 447–452.
34) V. Petříček, M. Dušek and L. Palatinus: Z. Kristallogr. **229** (2014) 345–352.
35) T. Matsumoto, A. Yamano, T. Sato, J.D. Ferrara, F.J. White and M. Meyer: J. Chem. Crystallogr. **51** (2021) 438–450.
36) G.M. Sheldrick: Acta Crystallogr. Sec. A **71** (2015) 3–8.
37) G.M. Sheldrick: Acta Crystallogr. Sec. C **71** (2015) 3–8.
38) A.W. Hull: Phys. Rev. **10** (1917) 661–696.
39) A.W. Hull: Phys. Rev. **17** (1921) 571–588.
40) L.-E. Edshammar: Acta Chem. Scand. **19** (1965) 2124–2130.
41) L.-E. Edshammar: Acta Chem. Scand. **19** (1965) 871–874.
42) K. Kitahara, H. Takakura, Y. Iwasaki and K. Kimura: Acta Crystallogr. Sec. E **79** (2023) 946–951.
43) S. Mi, S. Balanetskyy and B. Grushko: Intermetallics **11** (2003) 643–649.
44) H.A. Gobran, D. Heger and F. Mücklich: Int. J. Mater. Res. **96** (2005) 794–800.
45) J. Liu, C. Zhou and H. Wang: Calphad **72** (2021) 102239.
46) L. Perring, F. Bussy, J.C. Gachon and P. Feschotte: J. Alloy. Compd. **284** (1999) 198–205.
47) J.-L. Pouchou and F. Pichoir: *Electron Probe Quantitation*, ed. by K.F.J. Heinrich and D.E. Newbury, (Springer, Boston, MA, 1991) pp. 31–75. doi:10.1007/978-1-4899-2617-3_4
48) Y.Q. Liu, G. Shao and K.P. Homewood: J. Alloy. Compd. **320** (2001) 72–79.
49) Y. Du, K.H. Chen, J.C. Schuster, L. Perring, B.Y. Huang, Z.H. Yuan and J.C. Gachon: Int. J. Mater. Res. **92** (2001) 323–327.
50) L. Ivanenko, G. Behr, C.R. Spinella and V.E. Borisenko: J. Crys. Growth **236** (2002) 572–576.
51) H. Okamoto: J. Phase Equilibria Diffus. **27** (2006) 203.

52) J.L. Murray and A.J. McAlister: Bull. Alloy Phase Diagrams **5** (1984) 74–84.
53) H. Völlenkle: Monatsh. Chem. **105** (1974) 1217–1227.
54) A. Yamamoto: Acta Crystallogr. Sec. A **49** (1993) 831–846.
55) CSD 2287686 and 2287687 contain the supplementary crystallographic data for the C and C_4 phases, respectively. These data can be obtained free of charge from FIZ Karlsruhe via www.ccdc.cam.ac.uk/structures.
56) Y. Grin, K. Peters, U. Burkhardt, K. Gotzmann and M. Ellner: Z. Kristallogr. **212** (1997) 439–444.
57) R. Simura, K. Sugiyama, S. Suzuki and T. Kawamata: Mater. Trans. **58** (2017) 1101–1105.
58) H. Li and C. Fan: Crystals **9** (2019) 526.
59) K. Momma and F. Izumi: J. Appl. Crystallogr. **44** (2011) 1272–1276.
60) CSD 2287688 contains the supplementary crystallographic data for the χ' phase. These data can be obtained free of charge from FIZ Karlsruhe via www.ccdc.cam.ac.uk/structures.
61) R.N. Corby and P.J. Black: Acta Crystallogr. Sec. B **33** (1977) 3468–3475.
62) J. Roger, F. Bosselet and J.C. Viala: J. Solid State Chem. **184** (2011) 1120–1128.
63) H. Uryu, T. Yamada, K. Kitahara, A. Singh, Y. Iwasaki, K. Kimura, K. Hiroki, N. Miyao, A. Ishikawa, R. Tamura, S. Ohhashi, C. Liu and R. Yoshida: Adv. Sci. (2023) 2304546, in press.
64) V. Elser: Phys. Rev. B **32** (1985) 4892–4898.
65) C. Liu, E. Fujita, Y. Katsura, Y. Inada, A. Ishikawa, R. Tamura, K. Kimura and R. Yoshida: Adv. Mater. **33** (2021) 2102507.
66) C. Liu, K. Kitahara, A. Ishikawa, T. Hiroto, A. Singh, E. Fujita, Y. Katsura, Y. Inada, R. Tamura, K. Kimura and R. Yoshida: Phys. Rev. Mater. **7** (2023) 093805.
67) W. Steurer and S. Deloudi: *Crystallography of Quasicrystals*, (Springer, Berlin, Heidelberg, 2009) p. 295. doi:10.1007/978-3-642-01899-2